Chapter 7
Microsystems for Dispersing Nanoparticles

C. Schilde, T. Gothsch, S. Beinert, and A. Kwade

Abstract Typically in the production of nanoparticles via bottom-up syntheses, agglomerates or even strong aggregates are formed which have to be redispersed in a subsequent dispersion process. Especially for the processing and screening of aggregated highly potential and cost-intensive biotechnological or pharmaceutical products, microsystems are advantageous due to high stress intensities, narrow residence time distributions, and high reproducibility as well as low volume flow. Depending on the geometry and the operating conditions of dispersing units within microsystems, various stress mechanisms have an effect on the dispersion process. However, in contrast to emulsification processes, the effect of cavitation is disadvantageous for high-pressure dispersion processes and can be avoided by applying backpressure. For the characterization and optimization of the stress intensity distribution and stressing probability in microchannels at various operating conditions, microparticle image velocimetry (μPIV) as well as single- and two-phase CFD simulations are well suited.

7.1 Introduction

Since several years, the importance of nanoparticles as high potential additives increases continuously in numerous branches of industry, e.g., chemical, pharmaceutical, extractive, food, and dye industry. Due to their size of 1–100 nm in at least one direction in space [13], the large specific surface area and the high amount of reactive surface molecules nanoparticles are attributed by extraordinary properties

C. Schilde • T. Gothsch • S. Beinert
TU Braunschweig, Institut für Partikeltechnik, Volkmaroder Str. 5, Braunschweig 38104, Germany

A. Kwade (✉)
TU Braunschweig, Institut für Partikeltechnik, Volkmaroder Str. 5, Braunschweig 38104, Germany

PVZ—Center of Pharmaceutical Engineering, Technische Universität Braunschweig, Franz-Liszt-Str. 35 A, Braunschweig 38106, Germany
e-mail: a.kwade@tu-braunschweig.de

© Springer International Publishing Switzerland 2016

A. Dietzel (ed.), *Microsystems for Pharmatechnology*,
DOI 10.1007/978-3-319-26920-7_7

[77]. These properties are considerably different from the well-known macroscopic material properties. For this reason, using nanoparticles as additives in a process chain can be advantageous to enhance existing product properties or to generate completely new product properties, e.g., photocatalytic activity, catalytic activity, abrasion resistance, thermal and electrical conductivity, tensile strength, hardness, hydrophobicity, easy-to-clean effect, viscosity, and color strength. Apart from the traditional top-down processing of particles down to the nanoscale via stirred media milling [11, 27, 51, 52], chemical bottom-up processes such as crystallization, precipitation, or pyrolysis are typically used in industry because of economic reasons. Despite significant process optimization, the resultant particle characteristics are related in a complex way to the chemical and physical processes of the particle synthesis [53]. Hence, in most bottom-up production processes, agglomerates or even strong aggregates [13] are formed which have to be redispersed in a subsequent more or less intense dispersion process. With respect to the required particle or aggregate fineness rotor-stator systems, high-pressure or ultrasonic homogenizers, dissolvers, kneaders, stirred media mills, and other dispersing machines are suitable for this dispersion step [55, 56]. Hereby, high-pressure systems are typically characterized by a narrow residence time distribution, a relative accurate adjustment of the induced stress intensities and frequencies as well as a good reproducibility [48]. For microsystems, the high stress intensities, narrow residence time distribution, and high reproducibility as well as low volume flow could be advantageous, e.g., for processing of highly potential and cost-intensive biotechnological or pharmaceutical products [6, 17].

7.2 Dispersing of Nanoparticles

Typically in industrial mass production of nanoparticles via chemical synthesis, agglomerate or even strong aggregate clusters of primary particles are produced, which have to be redispersed in order to obtain the desired product fineness and properties. A classification of agglomerates, aggregates, and flocculates depending on the interaction forces between the primary particles and specific surfaces is summarized by Schilde et al. [52]. Depending on the aggregate/agglomerate structure, size, primary interaction, and stability, the resistance against fragmentation and the efficiency of the dispersion process differs strongly [8, 50]. The influencing factors on the dispersion process can be classified into the aggregate/agglomerate properties, the properties of the continuous phase, and the characteristics and operating parameters of the dispersing device (see Fig. 7.1 [59]):

- Aggregate/agglomerate properties: The strength of a particulate structure depends basically on the material, the structure, and the type and strength of particle–particle interactions [32, 54, 57–60]. Hence, the dispersion process is strongly affected by the material, size, and structure of the aggregate/agglomerate. Especially, nanoparticulate aggregates have a high strength due to the number and strength of solid bridges between the primary particles.

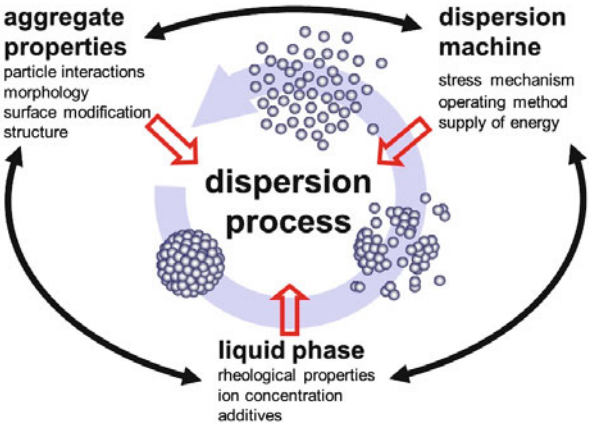

Fig. 7.1 Influencing parameters in a dispersion process (aggregate properties, dispersing machine, liquid phase) (original graphic by Schilde [59])

- Liquid phase: The properties of the continuous phase have an effect on the transferred stress frequencies and intensities by the dispersion machine [62] as well as on the suspension stability [37, 51, 78] concerning reagglomeration (rheological properties, ion concentration, additives, etc.).
- Dispersion machine: The stress mechanisms, intensities, and frequencies acting on aggregate/agglomerate surfaces depend considerably on the type, geometry, and operating conditions of the dispersing machine. In practice, dissolvers, high-pressure and ultrasonic homogenizers, kneaders, three roller mills as well as stirred media mills are used as dispersion devices [56].

7.3 Stress Mechanisms in Microsystems

A first principal classification of different stress mechanisms predominating the dispersion and comminution of particles in different dispersing machines was postulated by Rumpf [43, 52, 59]. The stress mechanisms were differentiated by the type of force transmission, e.g., compression or impact, stress by the surrounding fluid phase or thermal, chemical or electrical stresses. Apart from that the direction of energy initiation can be differentiated, e.g., normal or shear stress on a surface as well as shear or turbulent flow due to the fluid. A summary of different stress mechanism acting in different dispersing machines is given by Schilde et al. [52, 55]. For emulsification and dispersing in high-pressure systems, the hydrodynamic stresses acting on the particle and droplet surface due to pressure and velocity gradients are of major importance. Apart from particle–particle and particle–geometry interactions, the dispersion relevant stress mechanisms can be focused on stress via laminar and turbulent shear flow and stress via cavitation. The significance of these three stress mechanisms, especially the role of cavitation, on the emulsification result in high-pressure systems is not fully clarified and discussed controversially by different authors [18]. There are a large number of authors who

predict a positive effect of cavitation on the emulsification result [3, 15, 21, 31, 70, 71]. However, a large number of authors postulated a contrary minor or negative influence of cavitation on the emulsification result compared to laminar or turbulent shear flow [40–42, 67]. A few authors conclude that both turbulent shear flow and cavitation are the reasons for a successful breakup of droplets [24, 25].

While emulsification processes are intensely investigated regarding the effect of different mechanisms on the resultant product droplet size, only little literature exists on dispersing processes using high-pressure homogenizer or microsystems. However, similar to emulsification processes, it can be assumed that areas of high energy dissipation are responsible for a sufficient dispersion process. Sauter et al. identified hydrodynamic, cavitation, and impact stresses as effective stress mechanisms for dispersing pyrogenic nanoparticles [48, 49]. Anyway, cavitation leads to abrasion and damage and a reduced lifetime of the high-pressure systems. Thus, wear of the high-pressure homogenizer or microsystem has to be considered for dispersing in microsystems. Moreover, the dominant stress mechanisms in dispersing and emulsification processes differ considerably.

7.3.1 Stress via Laminar Fluid Flow

For Reynolds numbers below a critical value, laminar flow with only a marginal transverse flow can be observed [61]. This laminar flow can be differentiated into laminar shear flow [44] and laminar elongation flow [9, 20, 69] with different shear stresses acting on the particle surface. In general, both laminar shear and elongation flow occur simultaneously in a microsystem. Figure 7.2 shows the dominating stress mechanisms during dispersing of nanoparticulate suspensions in high-pressure and microsystems. Usually, in microsystems, these laminar shear and elongation stresses occur simultaneously but with various frequencies and intensities. For spherical particles in laminar shear flow of a Newtonian fluid, the shear stress and stress frequency acting on the particle surface can be calculated according to the following equation [44]:

$$\tau_{\mathrm{l,P,s}} = 2.5 \cdot \dot{\gamma} \cdot \eta_{\mathrm{f}} \tag{7.1}$$

$\tau_{\mathrm{l,P,s}}$	$\mathrm{N/m^2}$	Shear stress acting on the particle surface in laminar shear flow
$\dot{\gamma}$	1/s	Shear rate
η_{f}	$\mathrm{Pa \cdot s}$	Dynamic viscosity of the Newtonian fluid phase

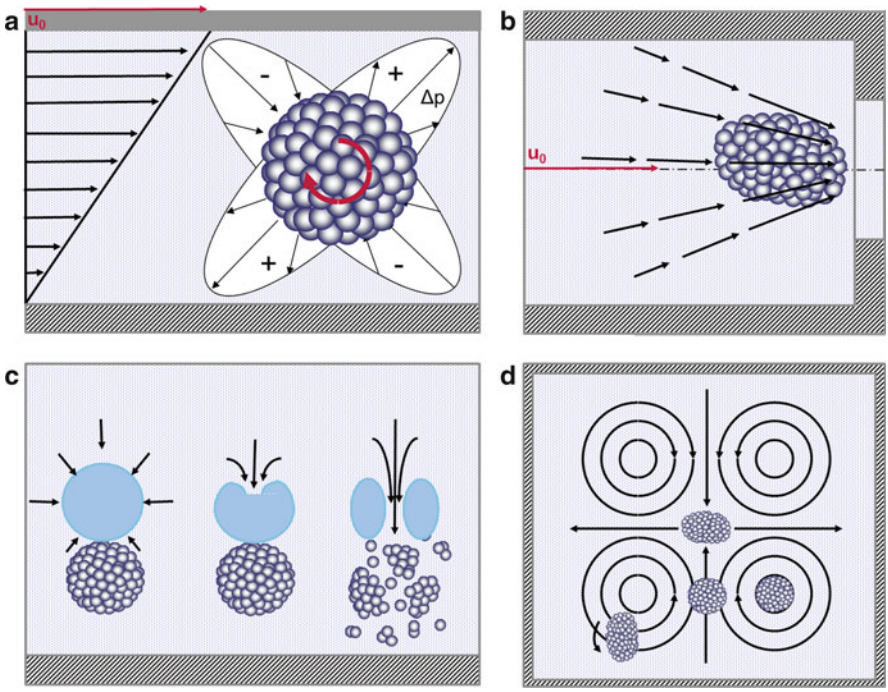

Fig. 7.2 Main stress mechanisms during high-pressure dispersing in microsystems: (**a**) laminar shear flow according to Rumpf [44]; (**b**) laminar elongation flow according to Stang [66]; (**c**) Cavitation; (**d**) turbulent shear flow according to the theory of Kolmogorov [12]

The stress frequency is proportional to the rotational angular velocity of the particle/aggregate within a stationary laminar shear flow:

$$\omega = \frac{\dot{\gamma}}{2} \tag{7.2}$$

ω	1/s	Angular velocity

Besides the shear stress acting on the particle surface, additionally centrifugal forces appear due to the rotation of the particle/aggregate within the stationary laminar fluid flow. However, the centrifugal forces are proportional to the square of the particle radius [44] and, thus, insignificant for dispersing small particles in the nanometer size range within microsystems. The elongation stress in laminar elongation flow is defined according to the following equation [33]:

$$\tau_{\mathrm{l,P,e}} = \dot{\varepsilon} \cdot \eta_{\mathrm{f}} \tag{7.3}$$

$\tau_{l,P,e}$	N/m^2	Elongation stress acting on the particle surface in laminar flow
$\dot{\varepsilon}$	1/s	Elongation rate

7.3.2 Stress via Turbulent Fluid Flow

In most cases, an accurate characterization of the three-dimensional flow and stress pattern is hardly available. Hence, computational fluid dynamics or mean field theories are suitable to describe the shear stress acting on the particle surface in turbulent shear flow. Turbulent shear flow is highly irregular, characterized by apparently random and chaotic three-dimensional eddies [16]. The energy is transferred by an eddy cascade and dissipated into energy of the smallest eddies with the Kolmogorov length scale due to dominating viscosity effects. In principle, the acting stresses can be classified using the ratio of the particle/aggregate and the Kolmogorov microscale into three to four classes [26, 29, 30, 38]:

- The inertial subrange, where the particles are stressed due to the relative velocities between vortices:

$$\tau_{t,P,isr} \sim \rho_f \cdot (\varepsilon \cdot d_P)^{2/3} \quad 25 \geq \frac{d_P}{\lambda_K} \geq 12 \tag{7.4}$$

$\tau_{t,P,isr}$	N/m^2	Turbulent stress in inertial subrange
ε	m^2/s^3	Energy dissipation rate
d_P	m	Particle/aggregate size
ρ_f	kg/m^3	Fluid density
υ_f	m^2/s	Kinematic fluid viscosity
$\lambda_K = \left(\frac{\upsilon_f^3}{\varepsilon}\right)^{1/4}$		Kolmogorov microscale

- The upper dissipation region, where the particles are stressed due to the relative velocities between vortices, but particle/aggregate diameter and kinematic viscosity have a higher influence on the acting stresses:

$$\tau_{t,P,uD} \sim \rho_f \cdot d_p^2 \cdot \frac{\varepsilon}{\upsilon_f} \quad 12 \geq \frac{d_P}{\lambda_K} \geq 3 \tag{7.5}$$

$\tau_{t,P,uD}$	N/m^2	Turbulent stress in the upper dissipation region

- The lower dissipation region, where the particles are stressed via rotation within the center of an eddy. The shear stress is independent on the particle/aggregate size. Typically, the ratio of the particle size and the Kolmogorov microscale for dispersing nanoparticle reaches values below 3 [55]:

$$\tau_{\mathrm{t,P,lD}} \sim \rho_{\mathrm{f}} \cdot (\varepsilon \cdot \upsilon_{\mathrm{f}})^{1/2} \quad \frac{d_{\mathrm{P}}}{\lambda_{\mathrm{K}}} \leq 3 \tag{7.6}$$

$\tau_{\mathrm{t,P,lD}}$	N/m^2	Turbulent stress in the lower dissipation region

Bache postulated an extended function for the lower dissipation region [2]:

$$\tau_{\mathrm{t,P,lD,\ Bache}} \sim \frac{1}{15} \rho_{\mathrm{f}} \cdot (\varepsilon \cdot \upsilon_{\mathrm{f}})^{\frac{1}{2}} \cdot \left(\frac{d_{\mathrm{P}}}{\lambda_{\mathrm{K}}}\right)^2 \quad \frac{d_{\mathrm{P}}}{\lambda_{\mathrm{K}}} \leq 3.5 \tag{7.7}$$

7.3.3 Stress via Hydrodynamic Cavitation

Typically, in literature, cavitation is discussed as a main stress mechanism during dispersion or emulsification processes using high-pressure or ultrasonic homogenizers [3, 5, 14, 21, 31, 35, 47, 63, 71]. Cavitation describes the spontaneous formation, growth, and subsequent collapse of cavities in a liquid phase. The previous nucleation process of cavities can be differed in homogeneous and heterogeneous nucleation. Due to thermal motion of liquid molecules, temporary, microscopic cavities arise which represent weak spots within the fluid and grow up, forming macroscopic cavities. This type of nucleation is called homogeneous nucleation. If the nucleation starts induced to already existing small gas bubbles or particles within the fluid phase, heterogeneous cavitation nucleation takes place. The implosion time and resultant velocities of the resultant cavities can be approximated according to Baldyga et al. [3]. The stress intensity of the microjet after implosion of the cavity can be described by the following equation [4]:

$$\tau_{\mathrm{j}} = \alpha \cdot \rho_{\mathrm{f}} \cdot c_{\mathrm{sw}} \cdot u_{\mathrm{j}} \tag{7.8}$$

τ_{j}	N/m^2	Stress intensity of the microjet
c_{sw}	m/s	Speed of shock wave
u_{j}	m/s	Speed of microjet
α	–	Empirical constant

In high-pressure systems, the hydrodynamic cavitation is generated due to high pressure gradients caused by high velocity gradients within the fluid flow. This cavitation can be differentiated into (1) travelling cavitation, (2) fixed cavitation,

(3) vortex cavitation, and (4) vibratory cavitation [64]. Furthermore, in microsystems which are based on orifice geometries, the cavitation regimes can be characterized similar to a quasi-stationary fluid flow:

- Beginning of the cavitation (cavitation inception).
- The steam fills the flow separation region (sub-cavitation stage).
- Expanding cavitation downstream (transitional cavitation) [46].

The amount of vapor-filled areas within the microsystem can be described using the cavitation number, e.g., [36]:

$$\mathrm{CN} = \frac{p_1 - p_3}{p_3 - p_\mathrm{v}} \tag{7.9}$$

CN	–	Cavitation number
p_1	N/m^2	Pressure upstream the orifice
p_3	N/m^2	Pressure downstream the orifice
p_v	N/m^2	Vapor pressure

As described before, the significance of laminar and turbulent shear flow and stress via cavitation is not fully clarified and discussed controversially by different authors. Typically, the presence of cavitation can be characterized using photo-optical measurement methods, e.g., for diesel injection nozzles [10, 45, 65, 68]. Figure 7.3 (left) shows exemplarily the visualization of cavitation in a rectangular silicon orifice [34] using a fluorescent dye with ambient pressure at the outlet of the microsystem [18, 19]. A dark blue color represents a low fluorescent intensity and, thus, cavities. The method is described in detail by Gothsch et al. [19]. The flow

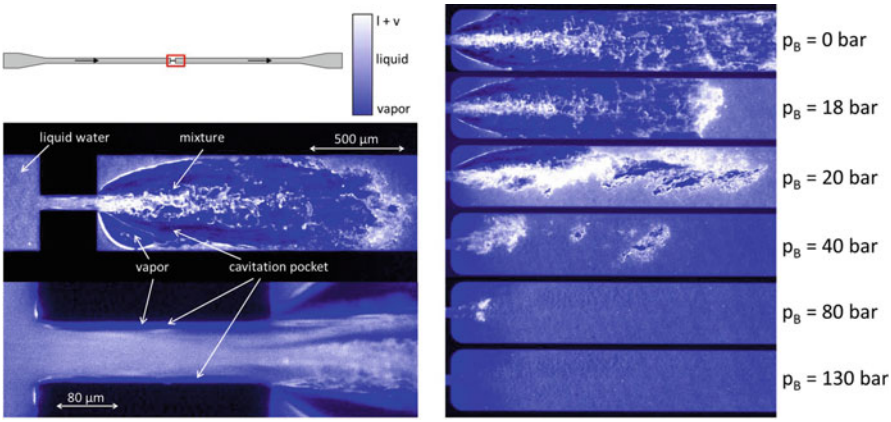

Fig. 7.3 *Left*: Cavitation images of a rectangular silicon orifice geometry ($\Delta p = 100$ bar; backpressure $p_\mathrm{B} = 0$ bar (ambient pressure); channel height $h_\mathrm{mc} = 53$ µm). *Right*: Cavitation downstream of the orifice at a pressure difference of 300 bar and increasing backpressure (original graphic by Gothsch et al. [19])

separation in the Vena Contracta as well as the detachment of the flow from the side walls forming cavitation pockets which propagate downstream can be described qualitatively. The fluid leaves the orifice as a jet with two fixed cavitation pockets next to it. In Fig. 7.3 (right), the effect of a backpressure on the reduction of downstream cavitation within the microsystem can be illustrated. In a first step, the fixed cavitation pockets collapse and small cavities can be observed in the region of the jet [1, 36]. Above a critical backpressure (130 bar at a pressure difference of 300 bar), cavitation is eliminated downstream of the orifice. The effect of cavitation on the product fineness dispersing pyrogenic alumina nanoparticles is discussed in Sect. 7.5.

7.4 Characterization of Fluid Flow in Microsystems

In principle, computational fluid dynamics as well as visual observations are well suited for the characterization of the fluid flow for dispersing nanoparticles at high pressures and small channel geometries of several tens of microns. However, high pressures and fluid velocities are a major challenge for the establishment of an experimental setup for visual observations of the fluid flow. Often sensors are integrated in the walls of the microchannels as an alternative experimental method [41]. However, the effect of these sensors on the fluid flow is unpredictable compared to the favored visual observations. As a result of the challenges associated with an experimental setup for visual observations, most investigations on dispersing particles/aggregates and formation of cavities within microsystems were conducted at larger channel geometry scales [1, 36, 39, 46, 63] or strongly reduced pressure gradients [22]. For this reason, the resultant observations regarding cavitation and dispersing phenomena differ strongly from those obtained at high pressures and small channel geometries. An opportunity to measure the velocity flow field within a microsystem at comparatively high pressures and small channel geometries is the usage of Microparticle Image Velocimetry (μPIV). Due to the high fluid velocities, small interframing times are necessary. In order to reduce the interframing time below the interframing time of a single CCD camera, the installation of two CCD cameras with matched internal shutters is necessary for the visual observations in microsystems with high fluid velocities. Figure 7.4 shows exemplarily the experimental setup of the μPIV for the characterization of fluid flow and cavitation within microsystems for high fluid velocities. Figure 7.5 shows exemplarily a cavitation image of a T-microchannel geometry at the conjunction without backpressure and a pressure difference of 200 bar (top) as well as the resultant flow field at a pressure difference of 500 bar and an additional backpressure of 60 bar to eliminate cavitation (bottom) [18, 19]. Fluid velocities of about 185 m/s were measured directly in the conjunction.

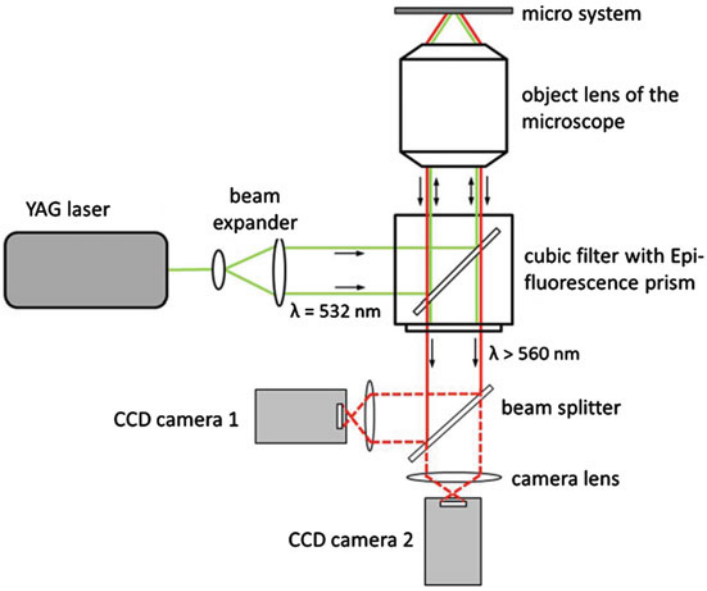

Fig. 7.4 Experimental setup of the μPIV for the characterization of fluid flow and cavitation within microsystems

7.5 High Pressure Dispersing in Microsystems

High-pressure systems are composed of a high-pressure device (e.g., pump) for pressure generation and a dispersing unit which expands the fluid to ambient pressure. Depending on the application, pressure differences between 20 and 4000 bar are realized [28]. Classically, radial diffusors consisting of valve seat and valve plunger are used as dispersing unit [63].

High-pressure homogenizers are predominantly used for emulsification processes, since dispersion of nanoparticulate suspensions demands higher stress intensities and frequencies for a successful reduction of the aggregate size as well as a higher abrasion resistance of the dispersion device. Figure 7.6 shows exemplarily the damage of an orifice dispersing unit due to cavitation and an abrasive nanoparticulate alumina suspension. Typically, the pressurized suspension is expanded abruptly to ambient pressure using a dispersing unit with a cross-sectional tapering. In front of the cross-sectional tapering, the fluid flow is characterized by a laminar elongation flow with superimposed laminar shear flow which changes to turbulent shear flow subsequent to the smallest cross-sectional area [28]. Furthermore, cavitation may occur due to abrupt changes in the microchannel geometry. Thus, several stress mechanisms for aggregate breakup described in detail in Sect. 7.3, i.e., stress via laminar shear and elongation and turbulent flow as well as stress via cavitation, take place simultaneously within or subsequent to the dispersion unit. Apart from other influencing factors (see Fig. 7.1), the dominating

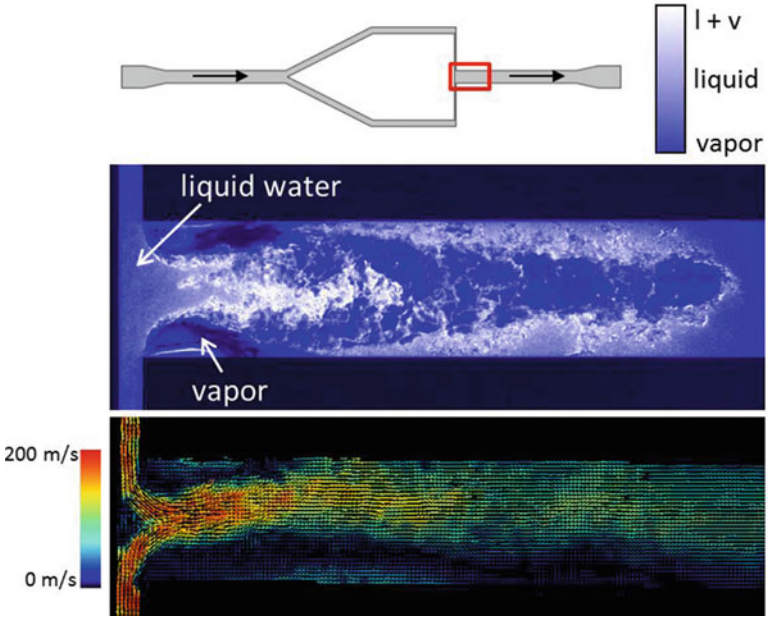

Fig. 7.5 *Top*: Cavitation images of the T-geometry at the conjunction ($\Delta p = 200$ bar; without backpressure $p_B = 0$ bar (ambient pressure); channel height of $h_{mc} = 53$ μm). *Bottom*: Flow measurement at a pressure difference of 500 bar and a backpressure of 60 bar using the μPIV setup shown in Fig. 7.4 (original graphic by Gothsch et al. [19])

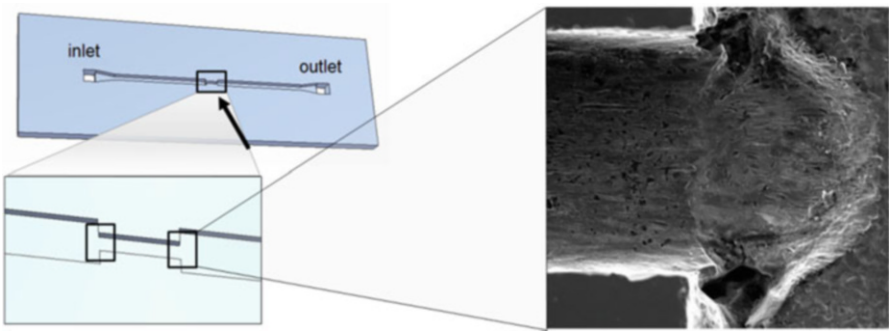

Fig. 7.6 Damage of a silicon orifice dispersing unit due to cavitation and an abrasive nanoparticulate alumina suspension

stress mechanisms as well as the product fineness of the dispersion process depend on the geometry of the dispersion unit, the suspension viscosity, the pressure difference, backpressure, and specific energy input. General statements regarding the dominating stress mechanisms are hardly possible. However, the effect of various process and formulation parameters on the product fineness can be identified, which are discussed in the following.

In general, only little literature exists on dispersing nanoparticles using high-pressure homogenizers or microsystems. Wengler et al. investigated the dispersion of nanoparticulate suspensions experimentally and via computational fluid dynamics using an orifice as dispersing unit [73–76]. According to Wengler et al. [72], elongation stresses exceed the stresses induced by turbulent shear flow. Moreover, laminar shear flow is negligible. The crucial stress mechanisms according to Sauter et al. are cavitation, impact, and hydrodynamic stresses [48, 49]. For an effective dispersion process, a high energy dissipation density is necessary. Moreover, according to Sauter et al., applying backpressure or a post-feeding of the nanoparticulate suspension directly behind the orifice is advantageous for the dispersion process.

7.5.1 Effect of the Microsystem Geometry

For cylindrical orifice dispersion units with orifice diameters between 80 and 300 μm, Sauter et al. [48] investigated the effect of impinging jets with different angles of the boreholes and an orifice with a subsequent impinging plate compared to a standard orifice configuration. The volume specific energy input to reach a certain product particle size was strongly decreased by using impinging orifice geometries. Moreover, the product fineness was increased using the impinging jet geometry and further increased by dispersing within impinging plate geometry. An increasing angle of the boreholes of the impinging jet geometry leads to increasing product fineness and energetic efficiency of the dispersion process. Apart from those crucial findings, these orifice dispersion units differ from classical microsystems.

Figure 7.7 shows exemplarily the effect of different dispersion geometries on the resultant median aggregate size of pyrogenic alumina as function of the number of passes through the microchannels (channel height of 26.6 μm and pressure difference of 500 bar) according to Gothsch et al. [19]. Although the differences in the resultant aggregate sizes are small, a clear trend of the dispersion efficiencies and maximum stresses between the different geometries can be derived. The highest dispersion efficiencies and stresses are provided by orifice geometries followed by the T-geometries, whereas straight and Z-channels lead to coarser particle sizes. Furthermore, significant differences within the same geometry type cannot be identified except for the orifice geometries.

The relative velocities of particle and fluid as well as the acting stresses within different microsystem geometries can be calculated from tracking the path of

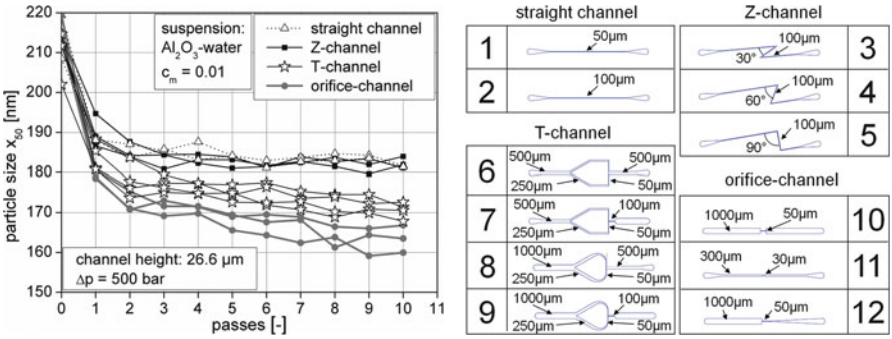

Fig. 7.7 Effect of the microsystem geometry on the dispersion result for rectangular microsystems with a channel height of 26.6 µm at a pressure difference of 500 bar and no backpressure (ambient pressure) (original graphic by Gothsch et al. [17])

particles with a certain diameter (230 nm) along the microsystem in a two-phase (liquid and gas) CFD simulation [7]. Figure 7.8 shows the maximum relative particle velocities for the abovementioned microchannel geometries at a pressure difference of 500 bar. Moreover, the velocity distribution within these geometries is shown. The relative velocities are an indicator for the stresses acting on the particle surface. The z- and straight channel geometries show a similar dispersion efficiency in the experiments (Fig. 7.7) which corresponds to the similar relative velocity distributions. The highest relative velocity distribution in the CFD simulation as well as the best dispersion efficiency is obtained for the orifice dispersion geometry. The T-channel (similar to the y-channel geometry) lays in-between (Figs. 7.7 and 7.8).

7.5.2 Effect of the Microsystem Height and Orifice diameter

The channel height of rectangular microsystems and the orifice width or diameter have a considerable effect on the dispersion process. Sauter et al. [48] investigated the effect of the orifice diameter on the resultant product fineness of dispersing nanoparticulate silica suspensions. As a result, the volume specific energy input for a certain product particle size increases strongly with decreasing orifice diameter. The dispersing unit with the smallest orifice diameter provides maximum product fineness.

Comparing the dispersion results of Figs. 7.7 and 7.9 with different channel heights, an increasing channel height leads to higher product fineness of all geometry types, except the orifice type. This corresponds to the results obtained by Sauter et al. [48] where a decreasing orifice diameter leads to an increasing product fineness. Main reason for the different effect of the channel height on the dispersing efficiency is the varying effect of the change in the cross-sectional areas on one hand and the change in the flow rate at a certain pressure drop on the other hand. A smaller channel height results in a higher fluid velocity if the volume flow rate stays

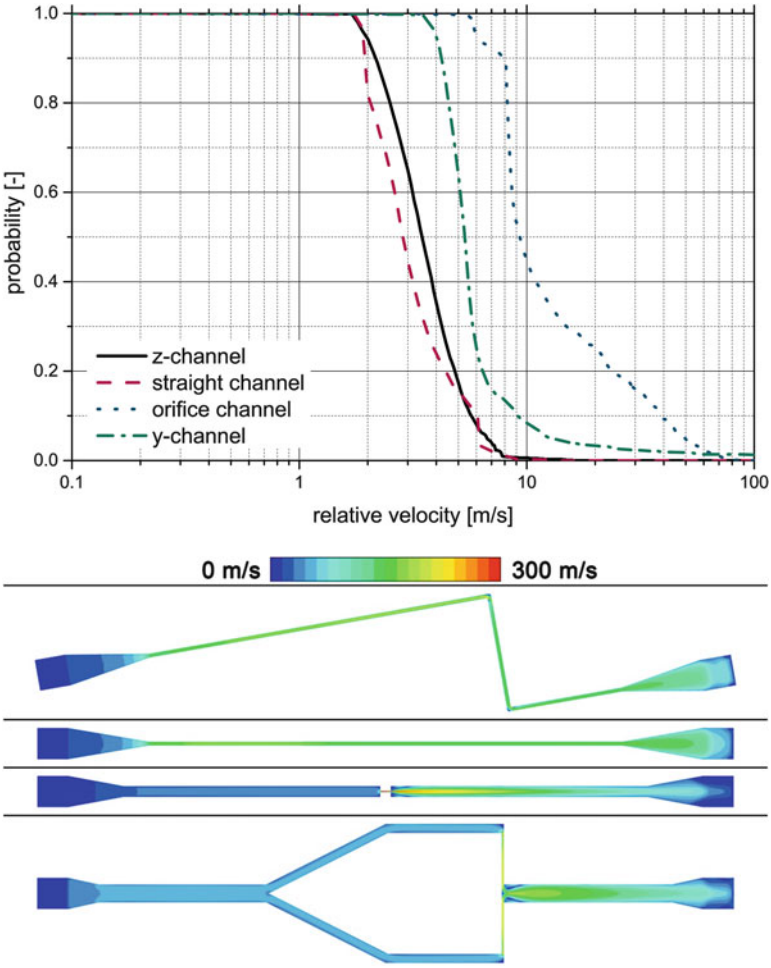

Fig. 7.8 Velocity distribution in the four different rectangular microsystem geometry types at a pressure difference of 500 bar obtained from two-phase CFD simulations (original graphic by Beinert et al. [7])

constant. However, the volume flow rate decreases due to a higher flow resistance at a constant pressure drop. A quantitative evaluation of the differences in the dispersion efficiencies, which are caused by various stress mechanisms, relative velocities, and stress distributions along the microchannels, can only be determined by Computational Fluid Dynamics (CFD) (e.g., by Beinert et al. [6, 7]).

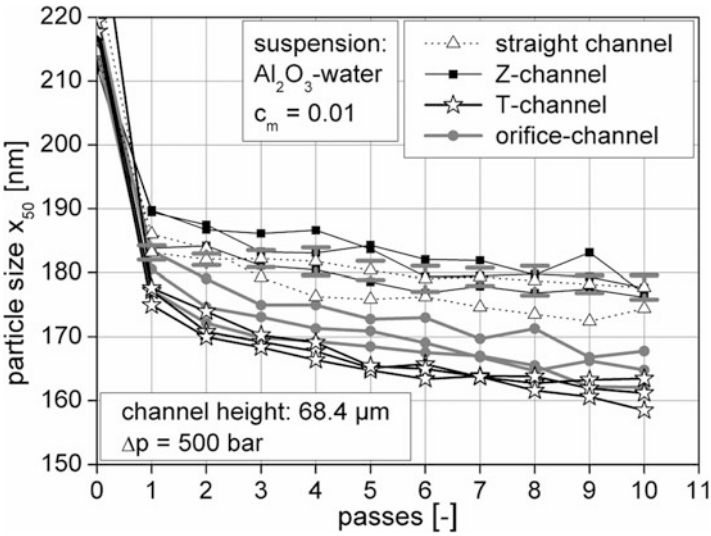

Fig. 7.9 Effect of microsystem geometry at a channel height of 68.4 µm on the dispersion result for rectangular microsystems at a pressure difference of 500 bar and no backpressure (ambient pressure) (original graphic by Gothsch et al. [17])

7.5.3 Effect of Cavitation

As mentioned before, the significance of the different stress mechanisms in microsystems, i.e., laminar and elongation shear flow, turbulent shear flow, and cavitation, especially the role of cavitation, on the dispersion is not fully clarified and discussed controversially by different authors. However, the importance of cavitation is solely discussed in context to emulsification processes or damage of microsystems. In emulsification processes a large number of authors predicted a positive effect of cavitation on the emulsification result [3, 15, 21, 31, 70, 71], a contrary minor or negative influence [23, 40–42, 67] or that both, turbulent shear flow and cavitation are the reasons for a successful breakup of droplets [24, 25]. The presence of cavitation can be characterized using photo-optical measurement methods shown in Fig. 7.3 and reduced or prevented by applying increasing backpressure [18].

The effect of cavitation on the dispersion efficiency was not clear and, thus, was investigated using an orifice geometry with different backpressures for dispersing pyrogenic alumina nanoparticles by Gothsch et al. (see Fig. 7.10). The cavitation was characterized via photo-optical measurements and visible at ambient pressure. Above 170 bar backpressure, no cavitation can be observed which is in good agreement with the results of a CFD simulation by Beinert et al. [7] which revealed the absence of cavitation at a backpressure of 170 bar. The dispersion efficiency of the orifice geometry increases by applying backpressure and, thus, by reducing and finally eliminating cavitation. Thus, cavitation does not contribute to the dispersion

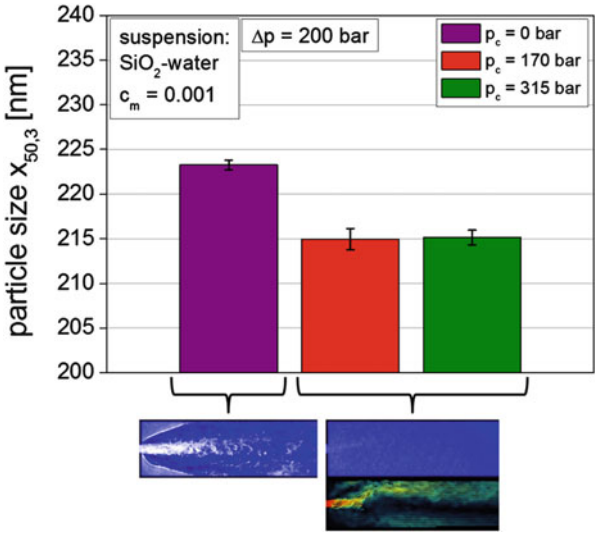

Fig. 7.10 Effect of cavitation on the dispersion efficiency at different backpressures for dispersing pyrogenic alumina nanoparticles (one pass at a pressure difference of 500 bar). Photo-optical measurements with visible cavitation at ambient pressure and photo-optical and μPIV measurements without cavitation above 170 bar backpressure

process but rather decreases dispersion efficiency in planar orifices. The effect of a backpressure on the volume flow rate as well as the dispersion efficiency is discussed in more detail at Gothsch et al. [18].

Highest shear stresses for dispersing within orifice channel geometries are just before and in the vena contracta. According to Beinert et al. [7], as long as the cavitation pockets in the orifice channel extend beyond the vena contracta, the volume flow rate should be reduced. Similar results are obtained by Gothsch et al. [18, 19] by investigating the effect of backpressure on cavitation and the volume flow. As mentioned before, the fluid volume flow stays constant independent of an increasing backpressure if cavitation is restricted to the area of flow detachment in the vena contracta. Figure 7.11 shows the experimentally measured and computed mass flow of an orifice microchannel geometry with and without backpressure. By applying backpressure and, thus, preventing cavitation the experimental mass flow data is in good agreement to the single-phase CFD simulations. Without backpressure and in the presence of cavitation, a two-phase CFD simulation is necessary to match the experimental measured and computed mass flow. Hence, CFD simulations can reproduce and predict cavitation and steam effects in microchannels. Figure 7.12 shows exemplarily the steam distribution in the different microchannel geometries without backpressure at a pressure difference of 500 bar.

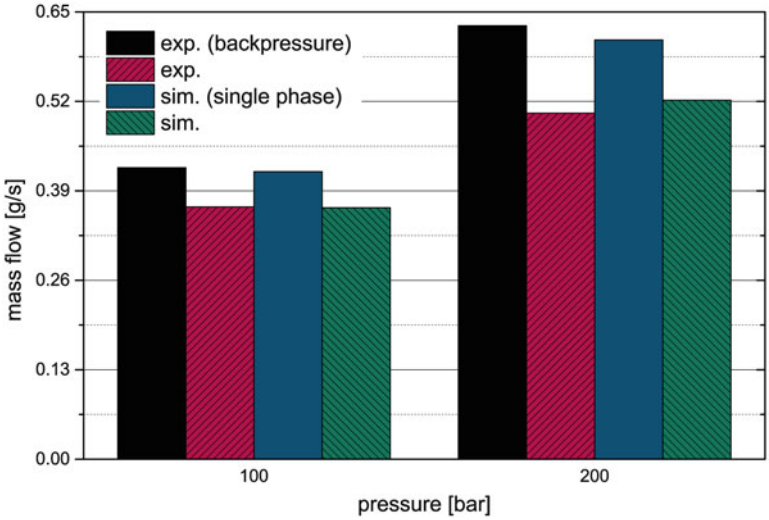

Fig. 7.11 Experimentally measured and computed (CFD simulations) mass flow for an orifice microchannel geometry with and without backpressure at two different pressure differences (original graphic by Beinert et al. [7])

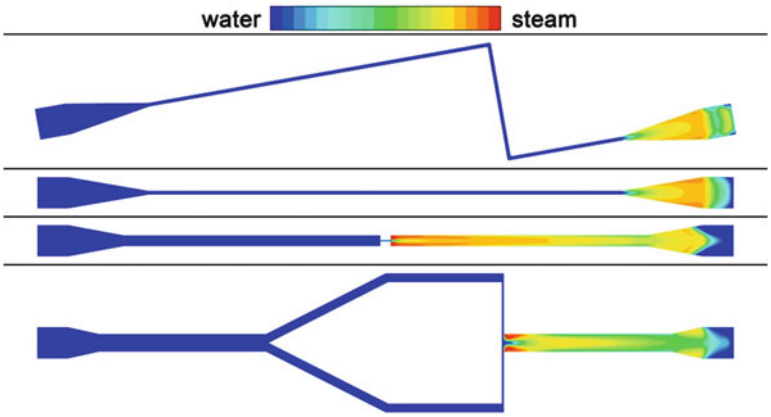

Fig. 7.12 Computed steam distribution in different microchannel geometries without backpressure at pressure difference of 500 bar (original graphic by Beinert et al. [7])

7.5.4 Effect of Number of Passes

For the breakage of aggregates and agglomerates within microsystems, the provided stress intensity of the dispersing unit has to be greater than the aggregate/agglomerate strength [6, 55]. Thus, the increase in product fineness depends on the maximum stress intensity, the stress intensity distribution as well as the stress frequency

or probability. Due to the fact that the aggregate strength typically increases with decreasing aggregate size and the maximum stress intensity provided by the dispersion unit of the microsystem is constant at constant operating conditions, a minimum aggregate/agglomerate size is obtained for infinite passes. Depending on the stress intensity distribution and stress frequency, the probability for each particle being stressed with the maximum stress intensity varies for each microchannel geometry. As an example, the maximum stress intensity within the straight and Z-channel geometry in Figs. 7.7 and 7.9 is comparatively low and greater particle sizes were reached. However, the probability that a particle experiences highest stress intensities is high and the maximum product fineness is reached after a few passes. In contrast, a further decrease of the particle size with increasing number of passes can be observed for the T- and the orifice channel due to a broad stress intensity distribution with small local areas of high maximum stresses.

To compare the dispersion efficiency of a dispersion process with a high number of passes with a single pass at much higher pressure differences, Fig. 7.13 shows a comparison of the dispersion via multiple passes and a single pass at various pressure differences as function of the volume specific energy input (according to Gothsch et al. [17]). Although the maximum stress intensity at a constant pressure difference stays constant and the probability that each particle is at least one time stressed by the maximum stress intensity increases with increasing number of passes, the dispersion efficiency via multiple passes at a lower pressure difference is limited by the maximum stress intensities. For increasing pressure differences, the stress intensity increases and a higher product fineness can be obtained. Hence,

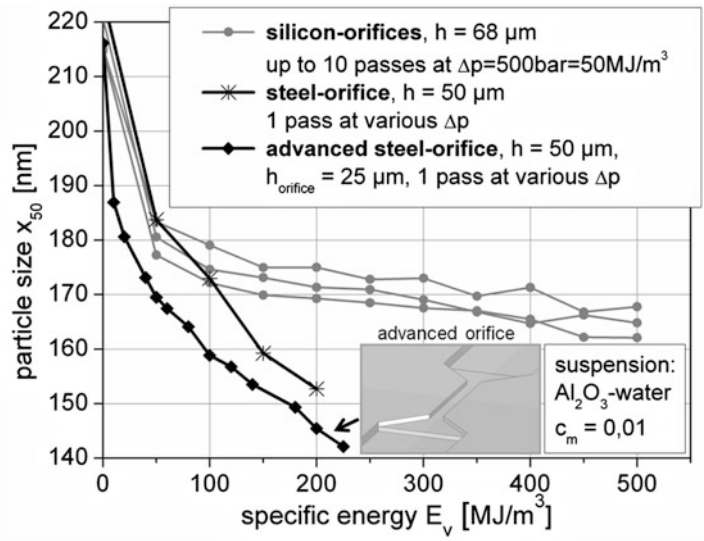

Fig. 7.13 Comparison of the dispersion process of multiple passes and a single pass at various pressure differences as function of the volume specific energy input (original graphic by Gothsch et al. [17])

higher pressure differences in a single pass are much more relevant for the dispersion of nanoparticles than multiple passes at a constant pressure difference. Moreover, Figure 7.13 shows the positive effect of an optimized orifice geometry with higher stress intensities on the dispersion efficiency.

7.6 Conclusion

Depending on the geometry and the operating conditions of dispersing units within microsystems, various stress mechanisms have got an effect on the dispersion process. In contrast to emulsification processes, the effect of cavitation is less important for high-pressure dispersion processes. Indeed, cavitation leads to damage of the dispersing units, reduces the volume flow, and leads to a less efficient dispersion of nanoparticulate suspensions. By applying backpressure, cavitation can be reduced and, thus, the volume flow increased and the dispersion efficiency of the dispersing unit increased. Furthermore, the usage of T-channels and especially orifice geometries as dispersing unit leads to high stress intensities and an increased dispersion efficiency. As a result depending on the target product fineness for application, the channel height or diameter has to be optimized. Moreover, in dispersion processes, a single pass at higher pressure difference is more efficient than dispersing multiple passes at a constant pressure difference. In summary, solid particles have a higher strength compared to droplets and are slightly deformable. Hence, emulsification and dispersing processes are hard to compare. Besides microparticle image velocimetry (μPIV), single- and two-phase CFD simulations (without and with cavitation) are well suited to characterize and optimize the stress intensity, stress distribution, and probability in microchannels. Moreover, the presence and effect of cavitation can be studied.

Acknowledgments The authors gratefully acknowledge the DFG for financial support within the DFG research group 856 “Mikrosysteme für partikuläre Life-Science-Produkte” (mikroPART).

References

1. Arai M, Shimizu M, Hiroyasu H (1985) Breakup length and spray angle of high speed jet. In: 3rd international conference on liquid atomization and spray systems (ICLASS), London
2. Bache DH (2004) Floc rupture and turbulence: a framework for analysis. Chem Eng Sci 59:2521–2534
3. Baldyga J, Makowski L, Orciuch W, Sauter C, Schuchmann HP (2008) Deagglomeration processes in high-shear devices. Chem Eng Res Des 86:1369–1381
4. Baldyga J, Orciuch W, Makowski L, Malski-Brodzicki M, Malik K (2007) Break up of nanoparticle clusters in high-shear devices. Chem Eng Proc 46:851–861
5. Behrend O, Schubert H (2001) Influence of hydrostatic pressure and gas content on continuous ultrasound emulsification. Ultrason Sonochem 8:271–276

6. Beinert S, Gothsch T, Kwade A (2012) Numerical evaluation of flow fields and stresses acting on agglomerates dispersed in high-pressure microsystems. Chem Eng Technol 35:1922–1930
7. Beinert S, Gothsch T, Kwade A (2015) Numerical evaluation of stresses acting on particles in high-pressure microsystems using a Reynolds stress model. Chem Eng Sci 123:197–206
8. Beinert S, Schilde C, Gronau G, Kwade A (2014) CFD-Discrete element method simulations combined with compression experiments to characterize stirred-media mills. Chem Eng Technol 37:770–778
9. Bentley BJ, Leal LG (1986) An experimental investigation of drop deformation and breakup in steady, two-dimensional linear flows. J Fluid Mech 167:241–283
10. Bergwerk W (1959) Flow pattern in diesel nozzle spray holes. Proc Inst Mech Eng 173:655–660
11. Breitung-Faes S, Kwade A (2008) Nano particle production in high-power-density mills. Chem Eng Res Des 86:390–394
12. Diekmann H, Metz H (1991) Grundlagen und Praxis der Biotechnologie: eine Einführung für Naturwissenschaftler und Ingenieure. G.Fischer, Stuttgart
13. DIN ISO/TS 27687:2010–02 (2010) Nanotechnologie—Terminologie und Begriffe für Nanoobjekte. Deutsches Institut für Normung e. V. (DIN)
14. Freudig B, Tesch S, Schubert H (2002) Herstellen von Emulsionen in Hochdruckhomogenisatoren—Teil 2: Bedeutung der Kavitation für die Tropfenzerkleinerung. Chemie Ingenieur Technik 74:880–884
15. Freudig B, Tesch S, Schubert H (2003) Production of emulsions in high-pressure homogenizers—Part II: influence of cavitation on droplet breakup. Eng Life Sci 3:266–270
16. George WK (2013) Lectures in turbulence for the 21st century. Chalmers University of Technology, Gothenburg
17. Gothsch T, Finke JH, Beinert S, Lesche C, Schur J, Büttgenbach S, Müller-Goymann C, Kwade A (2011) Effect of microchannel geometry on high-pressure dispersion and emulsification. Chem Eng Technol 34:335–343
18. Gothsch T, Richter C, Beinert S, Schilcher C, Schilde, Büttgenbach S, Kwade A (2016) Effect of Cavitation on Dispersion and Emulsification Process in High-pressure Microsystems (HPMS). Chemical Engineering Science (in press)
19. Gothsch T, Schilcher C, Richter C, Beinert S, Dietzel A, Büttgenbach S, Kwade A (2014) High-pressure microfluidic systems (HPMS): flow and cavitation measurements in supported silicon microsystems. Microfluidics Nanofluidics 18:121–130
20. Grace HP (1982) Dispersion phenomena in high viscosity immiscible fluid systems and application of static mixers as dispersion devices in such systems. Chem Eng Commun 14:225–277
21. Grob M (1951) Homogenisation von Milch und Milchkonzentraten mit einer Lavaldüse. Doctor PhD thesis, ETH Zürich, Zürich
22. Hakansson A, Fuchs L, Innings F, Revstedt J, Bergenstahl B, Trägardh C (2010) Visual observations and acoustic measurements of cavitation in an experimental model of a high-pressure homogenizer. J Food Eng 100:504–513
23. Mohr K-H (1980) Mechanismen der Hochdruckhomogenisierung, 1. Mitteilung: Turbulenz oder Kavitation als Zerkleinerungsmechanismen. Lebensmittelindustrie 27:399–403
24. Karbstein H (1994) Untersuchungen zum Herstellen und Stabilisieren von Öl-in-Wasser-Emulsionen. Dissertation, TH Karlsruhe, Karlsruhe
25. Karbstein H, Schubert H (1995) Developments in the continuous mechanical production of oil-in-water macro-emulsions. Chem Eng Proc 34:205–211
26. Kelly S (1999) Fluiddynamischer Einfluss auf die Morphogenese von Biopellets filamentöser Pilze. Institute of Biochemical Engineering, TU Braunschweig, Braunschweig
27. Knieke C, Steinborn C, Romeis S, Peukert W, Breitung-Faes S, Kwade A (2010) Nanoparticle production with stirred-media mills: opportunities and limits. Chem Eng Technol 33:1401–1411
28. Köhler K, Tesch S, Freudig B, Schuchmann HP (2012) Emulgiertechnik: Emulgieren in Hochdruckhomogenisatoren. Behrs Verlag, Hamburg

29. Kolmogorov AN (1958) Die lokale Struktur der Turbulenz in einer inkompressiblen zähen Flüssigkeit bei sehr großen Reynoldsschen Zahlen. Akademie Verlag, Berlin
30. Kolmogorov AN (1991) The local structure of turbulence in incompressible viscous fluid for very large Reynolds numbers. Proc Roy Soc Lond A 434:9–13
31. Kurzhals H-A, Reuter H (1979) Untersuchungen über die physikalisch-technischen Vorgänge beim Homogenisieren von Milch in Hochdruck-Homogenisiermaschinen. Chemie Ingenieur Technik 51:325
32. Kwade A, Schilde C, Burmeister CF, Roth M, Lellig P, Auerhammer GK (2013) Micromechanical properties of colloidal structures. Powders Grains 1542:939–942
33. Langer G, Deppe A (2000) Zum Verständnis der hydrodynamischen Beanspruchung von Partikeln in turbulenten Rührerströmungen. Chemie Ingenieur Technik 72:31–41
34. Lesche C, Gothsch T, Kwade A, Büttgenbach S (2011) Development of a dispersion micro-element for pharmaceutical screening applications: material and fabrication. In: Proceedings of MST Kongress 2011, Darmstadt, Germany, pp 642–645
35. Loo CC, Carleton WM (1953) Further studies of cavitation in the homogenization of milk products. J Dairy Sci 36:64–75
36. Martynov S (2005) Numerical simulation of the cavitation process in diesel fuel injectors. Doctor of Philosophy PhD thesis, University of Brighton, Brighton
37. Mende S, Stenger F, Peukert W, Schwedes J (2003) Mechanical production and stabilization of submicron particles in stirred media mills. Powder Technol 132:64–73
38. Niedballa S (1999) Dispergierung von feinen Partikelfraktionen in Gasströmungen—Einfluss von Dispergierbeanspruchung und oberflächenmodifizierenden Zusätzen. Faculty of Mechanical, Process and Energy Engineering, Technische Universität Bergakademie Freiberg, Freiberg
39. Payri R, Salvador FJ, Gimeno J, Venegas O (2013) Study of cavitation phenomenon using different fuels in a transparent nozzle by hydraulic characterization and visualization. Exp Therm Fluid Sci 44:235–244
40. Phipps LW (1971) Mechanism of oil droplet fragmentation in high-pressure homogenizers. Nature 233:617
41. Phipps LW (1974) Cavitation and separated flow in a simple homogenizing valve and their influence on the break-up of fat globules in milk. J Dairy Res 41:1–8
42. Phipps LW (1975) The fragmentation of oil drops in emulsions by a high-pressure homogenizer. J Phys D 8:448–462
43. Rumpf H (1959) Beanspruchungstheorie der Prallzerkleinerung. Chemie Ingenieur Technik 31:323–337
44. Rumpf H, Raasch J (1962) Desagglomeration in Strömungen. Symposium Zerkleinern, Weinheim
45. Salvador FJ, Martínez-López J, Caballer M, De Alfonso C (2013) Study of the influence of the needle lift on the internal flow and cavitation phenomenon in diesel injector nozzles by CFD using RANS methods. Energy Conv Manag 66:246–256
46. Sato K, Saito Y (2001) Unstable cavitation behavior in a circular-cylindrical orifice flow. In: Fourth international symposium on cavitation: CAV 2001, California Institute of Technology, Pasadena
47. Sauter C, Emin MA, Schuchmann HP, Tavman S (2008) Influence of hydrostatic pressure and sound amplitude on the ultrasound induced dispersion and de-agglomeration of nanoparticles. Ultrason Sonochem 15:517–523
48. Sauter C, Schuchmann HP (2007) High pressure for dispersing and deagglomerating nanoparticles in aqueous solutions. Chem Eng Technol 30:1401–1405
49. Sauter C, Schuchmann HP (2008) Materialschonendes Hochdruckdispergieren mit dem high pressure post feeding (HPPF)-system. Chemie Ingenieur Technik 80:365–372
50. Schilde C, Beinert S, Kwade A (2011) Comparison of the micromechanical aggregate properties of nanostructured aggregates with the stress conditions during stirred media milling. Chem Eng Sci 66:4943–4952

51. Schilde C, Breitung-Faes S, Kampen I, Kwade A (2013) Grinding kinetics of nano-sized particles for different electrostatic stabilizing acids in a stirred media mill. Powder Technol 235:1008–1016
52. Schilde C, Breitung-Faes S, Kwade A (2007) Dispersing and grinding of alumina nano particles by different stress mechanisms. Ceramic Forum Int 84:12–17
53. Schilde C, Gothsch T, Quarch K, Kind M, Kwade A (2009) Effect of important process parameters on the redispersion process and the micromechanical properties of precipitated silica. Chem Eng Technol 32:1078–1087
54. Schilde C, Burmeister C, Kwade A (2014) Measurement and simulation of micromechanical properties of nanostructured aggregates via nanoindentation and DEM-simulation. Powder Technol 259:1–13
55. Schilde C, Kampen I, Kwade A (2010) Dispersion kinetics of nano-sized particles for different dispersing machines. Chem Eng Sci 65:3518–3527
56. Schilde C, Mages-Sauter C, Kwade A, Schuchmann HP (2011) Efficiency of different dispersing devices for dispersing nanosized silica and alumina. Powder Technol 207:353–361
57. Schilde C, Westphal B, Kwade A (2012) Effect of primary particle morphology on the micromechanical properties of nanostructured alumina agglomerates. J Nanopart Res 14 (3):1–11
58. Schilde C, Kwade A (2015) Synthesis, structure and mechanics of nano-particulate aggregates. Springer, Switzerland
59. Schilde C (2012) Structure, mechanics and fracture of nanoparticulate aggregates. Institute of Particle Technology, TU Braunschweig, Braunschweig
60. Schilde C, Kwade A (2012) Measurement of the micromechanical properties of nanostructured aggregates via nanoindentation. J Mater Res 27:672–684
61. Schlichting H, Gersten K (2006) Grenzschichttheorie. Verlag G. Braun, Karlsruhe
62. Schröder C (2012) Rheologie- und Stabilitätseffekte bei der Nanozerkleinerung anorganischer Materialien. Institute of Particle Technology, TU Braunschweig, Braunschweig
63. Schuchmann HP, Danner T (2004) Emulgieren: Mehr als nur Zerkleinern. Chemie Ingenieur Technik 76:364–375
64. Shah YT, Pandit AB, Moholkar VS (1999) Cavitation reaction engineering. Kluwer Academic Plenum Publishers, New York
65. Sou A, Hosokawa S, Tomiyama A (2007) Effects of cavitation in a nozzle on liquid jet atomization. Int J Heat Mass Transf 50:3575–3582
66. Stang M (1998) Zerkleinern und Stabilisieren von Tropfen beim mechanischen Emulgieren. VDI-Verlag, Düsseldorf
67. Stang M, Schuchmann H, Schubert H (2001) Emulsification in high-pressure homogenizers. Eng Life Sci 1:151–157
68. Suh HK, Lee CS (2008) Effect of cavitation in nozzle orifice on the diesel fuel atomization characteristics. Int J Heat Fluid Flow 29:1001–1009
69. Taylor GI (1934) The formation of emulsions in definable fields of flow. Proc Roy Soc 29:501–523
70. Treiber A (1979) Zum Einfluss der Kavitation bei der Hochdruckhomogenisation von Öl-in-Wasser-Emulsionen. Dissertation, TH Karlsruhe, Karlsruhe
71. Treiber A, Kiefer P (1976) Kavitation und Turbulenz als Zerkleinerungsmechanismen bei der Homogenisation von O/W-Emulsionen. Chemie Ingenieur Technik 48:259
72. Wengeler R (2006) Hydrodynamic stress induced dispersion of nanoscale agglomerates by a high pressure process. PhD thesis, TH Karlsruhe, Karlsruhe
73. Wengeler R, Nirschl H (2004) Dispergierung nanoskaliger Agglomerate mittels Hochdruckver-fahren. Chemie Ingenieur Technik 76:1387–1388
74. Wengeler R, Nirschl H (2007) Turbulent hydrodynamic stress induced dispersion and fragmentation of nanoscale agglomerates. J Colloid Interface Sci 306:262–273
75. Wengeler R, Ruslim F, Nirschl H, Merkel T (2004) Dispergierung feindisperser Agglomerate mit Mikro-Dispergierelementen. Chemie Ingenieur Technik 76:659–662

76. Wengeler R, Teleki A, Vetter M, Pratsinis SE, Nirschl H (2006) High-pressure liquid dispersion and fragmentation of flame-made silica agglomerates. Langmuir 22:4928–4935
77. Yokoyama T (2007) Basic properties and measuring methods of nanoparticles: size effect and properties of nanoparticles, 1st edn. Elsevier, Amsterdam
78. Zellmer S, Grote C, Cheema T, Garnweitner G (2015) Colloid process engineering: small-molecule stabilization mechanisms of metal oxide nanoparticles. Springer, Switzerland, pp 73–91